Acetic acid ketonization on tetragonal zirconia. Role of surface reduction

Sergio Tosoni and Gianfranco Pacchioni*

Dipartimento di Scienza dei Materiali, Università di Milano Bicocca, via Cozzi 55, 20125 Milano, Italy

Version: 30.09.2016

Abstract

The ketonization reaction of acetic acid on the (101) surface of tetragonal zirconia, a process relevant in the catalytic upgrade of cellulosic biomass has been studied by means of DFT+U calculations. The aim is to better understand the role of catalyst pre-reduction. Acetic acid adsorbs strongly on the zirconia surface, and deprotonation to acetate takes place easily. Then, a proton transfer from the methyl group of the acetate ion, CH_3COO^-, to the surface occurs to form an eno-species, CH_2COO^{2-} (intermediate 1). In a parallel step, acetate ions convert into acyl fragments, CH_3CO, by oxygen extraction (intermediate 2). Once formed, the acyl intermediate 2 is able to attack the eno-species intermediate 1, to form a β-keto-acid. On stoichiometric zirconia, the formation of the intermediate 1, CH_2COO^{2-}, is unfavourable; oxygen vacancies on the reduced surface stabilize the reaction product and strongly reduce the activation energy. Reduced Zr^{3+} centres are essential to stabilize the acyl intermediate 2. The present work shows at an atomistic level the beneficial role of O vacancies and reduced Zr^{3+} centres for the ketonization process.

Graphical abstract

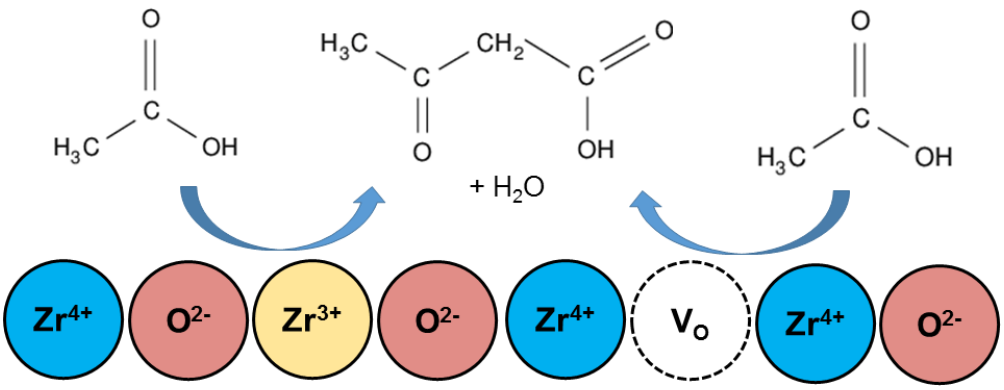

Highlights

- Ketonization occurs more easily on the surface of zirconia when this has been pre-reduced
- Reduction can occur via H_2 adsorption or H_2O desorption from an hydroxylated surface
- Reduction of ZrO_2 results in exposed Zr^{3+} ions or in point defects (oxygen vacancies)
- The reduced surface leads to more stable intermediates and lower activation barriers

Keywords

Ketonization, oxide surfaces, zirconia, oxygen vacancy, density functional theory

1. Introduction

In a general frame characterized by a growing demand of fuels derived from renewable sources, lignocellulosic biomasses represent a key-material for future development in fuels chemistry. A fundamental step in the biomass upgrading process consists in the elongation of the C-chain length and the reduction of the oxygen content of the raw material [1-3]. This can be achieved by pyrolysis of large volumes of biomasses [4] or, more efficiently, by promoting catalytically the condensation of short-chain carboxylic acids with elimination of water [1]. In pyrolytic processes, the dominant reaction to reduce the oxygen content of the biomass is the unimolecular decarboxylation [5]; for the case of acetic acid this results in the formation of CH_4 and CO_2. Differently, on heterogeneous catalysts such as oxide surfaces, several reactions take place, such as reduction of the carboxylic acids to aldehydes or ketonization [6,7]. Ketonization is a process where two carboxylic acids condense to form a ketone, eliminating H_2O and CO_2. The mechanisms of the ketonization reaction and the role of the heterogeneous catalysts have been extensively reviewed [8,9]. On oxide surfaces, in particular, the important role of undercoordinated cations and the presence of reduced centres are assumed to have a strong influence on the reactivity towards carboxylic acids [10,11]. Particular attention is devoted in the literature to the role of zirconia surfaces in biomass upgrading [12-18]. In this context, zirconia has been shown to be more effective in ketonization compared to other oxides widely employed in heterogeneous catalysis, such as ceria, silica or alumina [15]. Usually, the oxide catalyst (ZrO_2, TiO_2, etc.) is prepared by pre-treatment in hydrogen, a process that was shown to increase considerably the activity [8,18,19,20].

As discussed by Pulido et al [15], two mechanisms have been proposed in the literature for ketonization: a concerted mechanism [21, 22], and a step-wise mechanism implying the formation of a β-keto-acid intermediate [23]. The β-keto-acid mechanism has been studied in detail also on oxide surfaces [6,15,19,20,24]. Starting from two acetic acid molecules, the concerted mechanism implies the simultaneous formation of a C-C bond and decarboxylation, forming acetone and CO_2. The elementary steps of the initial phases of the step-wise mechanism, α-hydrogen abstraction and C-C coupling, are depicted in Scheme 1. These are followed by C-C scission with CO_2 formation and enolate hydrogenation to form acetone (not shown). In step a), an acetic acid molecule is adsorbed on zirconia, forming an acetate ion and a hydroxyl group grafted on the surface. The adsorbed acetate ion is further subjected to the enolization reaction (step b1), where a proton from the methyl group is transferred to the surface, forming a hydroxyl and a 1,1-ene-diolate species (intermediate 1). Alternatively (step b2), the acetate molecule undergoes deoxygenation, forming an

acyl species (intermediate 2) and an OH^- group bound to a surface cation. The importance of the acyl intermediate in the reaction has been recently shown for the case of HZSM-5 [25]. In step c, the enolate and acyl intermediates 1 and 2, respectively, combine to form a β-keto-acid ion, namely the 3-oxo-butyrrate in case of acetic acids reaction.

Of course, other reaction paths are also possible. For instance, the CH_2COO^{2-} intermediate 1 may directly attack a carboxylate fragment, CH_3COO^-. In other words, while it is rather well established that CH_2COO^{2-} is the key intermediate for C-C coupling, this is not necessarily the case for the CH_3CO species.

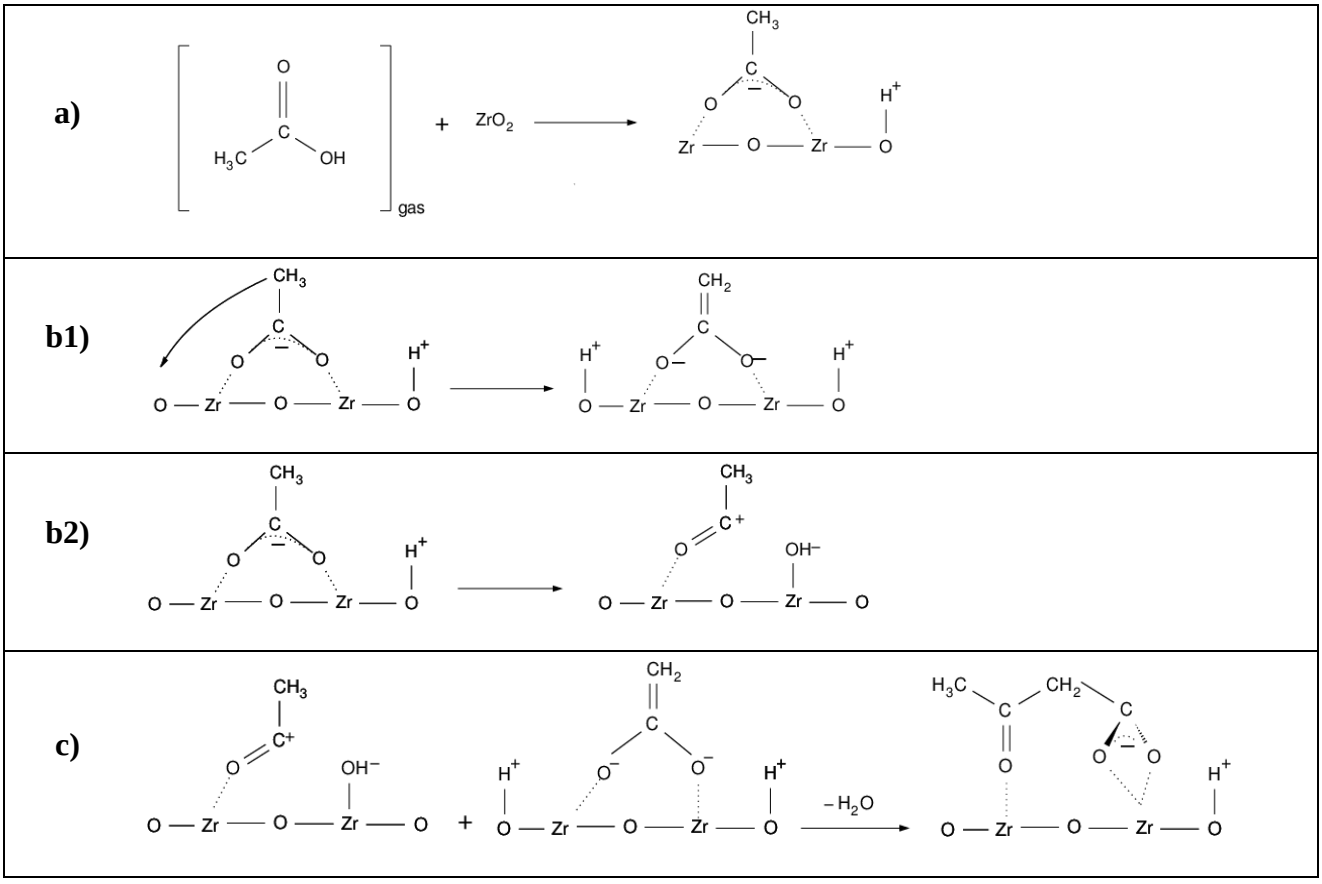

Scheme 1. Elementary steps of ketonization on the zirconia surface: a) adsorption of acetic acid, b1) formation of the enolate intermediate 1, b2) formation of the acyl intermediate 2, c) reaction of acyl and enolate to form the β-keto-acid.

According to DFT calculations on acetic acid ketonization on monoclinic zirconia (m-ZrO_2), the β-keto step-wise mechanism is kinetically favorable [15]. Moreover, experiments on the

ketonization of isomeric pentanoic acids showed that the abundance ratio of the products could not be explained according to the concerted route, further supporting the β-keto mechanism [15]. Once the 3-oxo-butyrrate is formed, a further reaction cleaves the C1-C2 bond with the hydrogenation of the methylene bridge, forming acetone and carbon dioxide. As shown by DFT calculations, this step is endothermic on m-ZrO_2 [15].

Thus, the catalytic activity of zirconia in biomass conversion has already been at the center of several investigations which have helped to elucidate the reaction mechanism. Looking at the elementary steps of the most plausible mechanism, it is clear that the capability of the support to act as an electron acceptor or donor is of paramount importance for three aspects: i) the acid-base equilibrium regulating the adsorption and deprotonation of acetic acid; ii) the charge transfer process in the acetate-enolate tautomeric equilibrium; and iii) the deoxygenation reaction that forms the acyl species. What still has to be better understood, is the role of the chemical reduction of the catalyst in the whole process [9]. In particular, the presence of reduced centers on the zirconia support seems to have a very strong impact on its reactivity [18]. This is the goal of the present investigation.

Zirconium dioxide is a wide-gap insulator that displays a complicated polymorphism. At room temperature, the most stable phase is the monoclinic one. At 1480 K, a phase transition to the tetragonal (t-ZrO_2) structure is observed. The latter finally converts into the cubic polymorph at the temperature of 2650 K [26]. The adsorption and reactivity of carboxylic acids on the surface of the most stable monoclinic phase has been thoroughly studied by means of DFT calculations [8,15,27]. The stabilization of the cubic and tetragonal phases down to room temperature is obtained by incorporating a small amount of impurities, in particular divalent or trivalent cations [28,29,30]. Tetragonal ZrO_2 exhibits excellent thermal and mechanical properties [31,32] but it has been less studied both experimentally and theoretically in relation to ketonization compared to the monoclinic one. Experimentally, a comparison of the activity of m-ZrO_2 with t-ZrO_2 has been reported in a few studies [18,33,34], and there is some evidence that the monoclinic phase may be more active than the tetragonal one [18]. In some cases the reaction has been studied on mixed tetragonal and monoclinic phases [35]. On both m-ZrO_2 and t-ZrO_2 a positive effect on ketonization of carboxilic acids was observed when the amount of surface coordinatively unsaturated Zr^{4+} cations is high and also when the catalysts are pre-treated with H_2. This has been justified with the appearance of Zr^{3+} cations on the ZrO_2 surface [33,34]. In the present work, we decided to concentrate on the tetragonal phase (t-ZrO_2), studying its most stable surface, i.e. the (101) [36], since, so far, this

phase has been much less investigated at theoretical level. Furthermore, mixed oxide catalysts such as CeO_2-ZrO_2 [33,34], resulting in improved performances in ketonization reactions, are dominated by tetragonal zirconia nanocrystals, thus providing additional motivations for the study of this phase.

As mentioned above, the reactivity of zirconia towards carboxylic acids is influenced by factors such as the intrinsic Lewis basicity of the surface cations, their undercoordination, and the presence of reduced centers. In a recent work, we studied the surface basicity of t-ZrO_2, simulating the adsorption of CO_2: CO_2 tends to be strongly chemisorbed on zirconia surfaces, with spontaneous formation of carbonate species, thus evidencing a pronounced tendency to bind carboxylates and carboxylic acids (CO_2 extracts an O ion from the lattice to form an adsorbed CO_3^{2-} species) [37]. Since the ketonization reaction implies the formation of CO_2, this could contribute to deactivate the surface. As far as the undercoordinated cations are concerned, zirconia stepped surfaces, exposing Zr^{4+} ions [38], display comparable basicity to the regular sites [37].

Zirconia is a scarcely reducible oxide, with the cost of creation of an oxygen vacancy close to 5.5-6 eV (computed with respect to the removal of ½O_2) [39]. However, other processes contribute to reduce the cost of creation of O vacancies. As recently shown, supported Ru [40] or Ni [41] metal particles strongly facilitate the creation of oxygen vacancies by promoting reverse oxygen spillover from the lattice to the metal particle. Another important path towards reduction of zirconia is adsorption of hydrogen, with formation of surface OH groups and Zr^{3+} ions [42]. In small zirconia nanoparticles (of size of about 2 nm) the cost of formation of O vacancies is also lower than on the regular surface [43]. In general, nanostructuring zirconia in form of nanoparticles helps considerably its reducibility. In this process, supported metal particles play a fundamental role, promoting the dissociation of H_2 molecules and the spillover of H atoms from the cluster to the support [19,20,44].

In the present work, we study the adsorption, enolization and ketonization reactions of acetic acid on t-ZrO_2 (101). The main goal is to provide a microscopic interpretation of the role of reduced centers at the surface of zirconia in ketonization. So far the reaction has been studied theoretically only on regular, non reduced surfaces. It is generally assumed that reduction of the zirconia catalyst results in exposed Zr^{3+} ions and that these are the reactive centers [34]. In the work of Peng et al. [35] it was suggested that ketonization of palmitic acid to palmitone is promoted by the presence of a surface oxygen vacancy, but a direct proof of this is lacking. Our study wants to provide atomistic insight into the role of surface reduction. Reduced centers on the zirconia supports are modeled by

considering (a) hydrogenated surfaces or (b) oxygen deficient surfaces, ZrO_{2-x}. There is a substantial difference between these two situations. Reduction in hydrogen results in an adsorbed proton and an excess electron that reduces a Zr^{4+} ion to Zr^{3+} without implying a change in the morphology of the surface. Oxygen removal, on the other hand, results in a morphological defect (oxygen vacancy) and in an electronic modification due to the formation of trapped electrons. These two situations can be distinguished by theory while they are hardly accessible experimentally. The choice of CH_3COOH as a model for carboxylic acids allows to reduce the complexity and the number of degrees of freedom of the problem. However, as proven by the systematic work of Ignatchenko in the case of the enolization reaction on m-ZrO_2 [27], differently substituted R-COOH molecules display similar activation energies, where the effect of the substituent R is as small as a few kcal/mol. We can therefore assume that acetic acid is a reasonable prototype for carboxylic acids.

2. Computational Details

All the calculations hereby reported are performed with the VASP 5 simulation package [45]. The electronic structure is calculated using the PBE exchange-correlation functional [46]. Valence electrons, i.e. H(1s), C and O(2s, 2p) and Zr(4s, 5s, 4p, 4d) are expanded on a set of plane waves with a kinetic cutoff of 400 eV, while core regions are treated with pseudopotentials, as encoded in the Projector Augmented Wave approach [47,48].

To improve the description of the electronic structure of zirconia, partial occupations of Zr d-orbitals are penalized by a Hubbard parameter, which has been empirically set to 4 eV (GGA+U approach) [49,50]. The long-range dispersion interactions are added according to the DFT+D2' semi-empirical approach. This scheme slightly modifies the original parameterization proposed in the DFT+D2 method by Grimme [51]. As recently shown [52], this approach provides reasonably accurate results in describing zirconia surfaces when compared to more complex and resource-intensive methods, such as the vdW-DF functional.

The (101) surface of tetragonal zirconia is modelled with a 3x2 supercell which contains 60 Zr and 120 O atoms. All surface oxygens are equivalent and have the same basicity. The slab has a thickness of five layers. An empty space of 15 Å is included in the cell to avoid spurious interactions between replicas.

Full structural relaxations are performed with convergence criteria of 10^{-5} eV and 10^{-2} eV/Å for the electronic and ionic loops, respectively. A kinetic energy cutoff of 400 eV is adopted. The

sampling of the reciprocal space is limited to the Γ-point.

Transition states are identified with the Nudged Elastic Band (NEB) method [53,54]. The reaction path is sampled with four images. The saddle point along the path is identified using the climbing NEB approach [55]. The structures are then characterized as transition states by means of harmonic frequency calculations.

The stability of any species X adsorbed on the surface, either minima or transition state, is calculated as the binding energy with respect to the gas-phase CH_3COOH molecule and the clean zirconia surface: $E_b\ (X) = E(X/ZrO_2) - E(CH_3COOH)_{gas} - E(ZrO_2)$.

3. Results and Discussion

3.1 Non-reduced t-ZrO_2 (101) surface

The energy profile of the adsorption of acetic acid on zirconia is shown in Fig. 1. The adsorption of acetic acid in molecular form in a tridentate configuration implies an energy gain of -1.92 eV with respect to the gas-phase CH_3COOH molecule and the clean surface. Other structures, such as a bidentate molecule, are higher in energy. Of course, the adsorption energy of -1.92 eV does not take into account entropy effects. These can be accounted for in an approximate way when gas-phase species are involved in the reaction, as suggested by Norskov [56]. The Gibbs free energy for adsorption is defined as $\Delta G_{ads} = \Delta H_{ads} - T(S_{ads} - S_g)$, where ΔH_{ads} is the enthalpy of adsorption approximated, in absence of mechanical work, by the corresponding change in total energy, T is the absolute temperature (573 K in our case, the reaction temperature), S_{ads} is the entropy of the adsorbed species, and S_g is the entropy of the gas-phase molecule. S_{ads} has been computed taking into account only the vibrational contributions to the partition function; S_g has been computed taking into account translational, rotational and vibrational contributions and is very close to the experimental standard molar entropy of CH_3COOH. With this approach, we computed a $T\Delta S_{ads}$ contribution of 1.19 eV which results in a ΔG_{ads} = -0.73 eV, still negative.

A proton transfer from the adsorbed CH_3COOH molecule to a three-coordinated surface O^{2-} ion leads to an acetate ion coordinated to the surface in a tridentate configuration. The proton transfer induces the displacement of a lattice O ion and the formation of an OH^- ion adsorbed on a surface Zr^{4+} cation and a surface vacancy. A similar high reactivity of surface oxide anions on the (101) surface of zirconia has been observed in CO_2 adsorption [37]. A moderate energy gain (0.12 eV) is associated to the proton transfer, indicating that dissociative adsorption is slightly preferred. The reaction barrier is rather small (+0.23 eV). A subsequent rearrangement of the acetate species

from tridentate to bidentate configuration is associated to an additional gain in stability from -2.04 eV to -2.34 eV. The kinetic barrier from the tridentate to the bidentate configuration has not been calculated, but it should be negligible, since it does not imply any breaking of covalent chemical bonds. Notice that it has been shown that entropy contributions to transition states with respect to reactants are negligible [57].

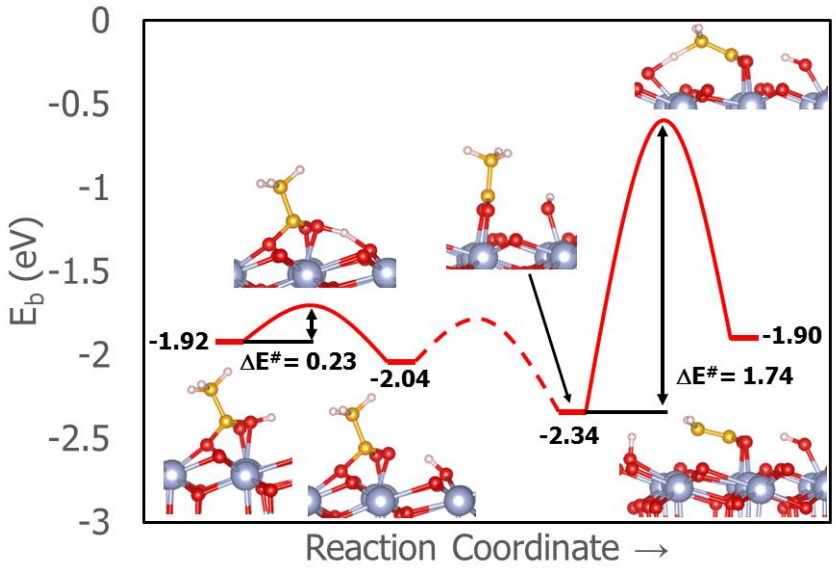

Fig. 1. Energy profile of acetic acid adsorption and enolization reaction on stoichiometric t-ZrO_2. Blue: Zr; red: O; yellow: C; white H. Energies in eV (computed with respect to a gas-phase acetic acid molecule).

As indicated in Scheme 1, the acetate can undergo an enolization reaction, transferring one proton from the CH_3 group to the surface (Fig. 1). This is considered to be a key step in the reaction (intermediate 1). The H-C-H angle goes from 108-111° in the acetate's methyl group to 117° in the methylene terminal group of the eno-form. Conversely, the C-C distance is shortened from 1.50 Å (acetate, single bond) to 1.40 Å (enolate, double bond). The C-O bonds are stretched from 1.28 Å to 1.34 Å passing from the carboxylate end of the acetate ion to the di-alkoxide end of the enolate. A change in the formal charge from -1 (acetate) to -2 (enolate) is also expected and is confirmed by

the Bader charges: -0.72 |e| acetate, -1.35 |e| enolate. It is also worth noting that the adsorbed acetate ion maintains a vertical arrangement on the surface, while the enolate lies flat, Fig. 1.

As shown in Fig. 1, on the stoichiometric surface the enolization reaction is an uphill process, and the reactants (E_b= -2.34 eV) are about 0.4 eV more stable than the products (E_b = -1.90 eV). What makes the reaction possible only at high temperatures, however, is the activation barrier which is rather high, +1.74 eV. In the transition state, the C-C bond has an intermediate length of 1.45 Å, while a proton is shared between the C atom of the adsorbed molecule and a lattice oxygen of the zirconia surface, with C-H and O-H distances of 1.40 Å and 1.36 Å, respectively. We explored also another possible transition state structure where the proton is transferred to an oxygen ion closer to the adsorbed molecule; the activation energy, however, does not change, +1.73 eV. One reason for this rather unfavourable activation energy is that both TS structures are remarkably distorted: in the structure reported in Fig. 1, there is an evident protrusion of a surface oxygen from its lattice position, while in the other TS structure the acetate ion is twisted. Calculations on the same reaction on monoclinic ZrO_2 (-111) led to a remarkably smaller activation barrier for enolization (+1.08 eV) [27]. This difference may be due either to the different morphology of monoclinic and tetragonal zirconia surfaces, or to the different computational schemes adopted (PBE+U+D2' in the present work, PW91 in ref. 27). In order to clarify the issue we have computed the initial, final and TS structures using three different computational approaches: PBE+U+D2', PBE+U, and PW91, Table 1. In this way we can distinguish the role of dispersion forces and of the exchange-correlation functional (with or without self-interaction correction) in determining the barrier for H abstraction. The results are very interesting as they show that dispersion has little effect, while at the PW91 level the barrier is much smaller, and is close to that reported by Ignatchenko for the monoclinic surface [27]. The PW91 functional tends to bind the products more strongly, leading to a thermoneutral reaction, with consequent strong decrease of the barrier, Table 1. These results have been obtained without re-optimizing reagents, products, and transition states, but nevertheless they clearly show (1) the importance of the choice of the functional in determining the energy profile, and (2) that using the same computational method the barriers are similar for monoclinic and tetragonal zirconia surfaces.

Table 1 – Role of computational method in determining the reaction profile in enolization reaction on tetragonal zirconia (energies in eV)[a]

	PBE+U+D2'	PBE+U	PW91
Reactants	0.0	0.0	0.0

Transition state	1.74	1.90	1.03
Products	0.44	0.66	0.04

[a] The calculations have been performed using the geometries of the stationary points obtained at the PBE+U+D2' level and recomputing the total energies.

As depicted in Scheme 1, step b2, a second path involves the formation of a positively charged acyl species, CH_3CO^+ (intermediate 2), where a concerted reaction of an O atom of CH_3COO^- with a surface proton leads to an OH^- group bound to a Zr ion. On tetragonal zirconia, however, stabilizing the acylium ion did not succeed because this fragment is extremely oxygen and electron deficient and induces the displacement of a surface O ion to re-create the CH_3COO^- unit and an O vacancy, formally in +2 charge state. This has been found also starting directly from an adsorbed undissociated acetic acid molecule: when we detach an OH^- group from CH_3COOH forming CH_3CO^+ (acylium ion) and a Zr-OH^- center, we observe the spontaneous displacement of an O ion from the surface towards the acylium with formation of an adsorbed acetate. This suggests that the positively charged CH_3CO^+ fragment cannot form on the surface of regular zirconia and does not allow the prosecution of the reaction, as depicted in Scheme 1, which necessarily implies the breaking of a carboxylic C-O bond. We also checked the possibility that the reaction proceeds via homolytic splitting of the C-O bond and formation of radical species ($CH_3CO^\bullet$ + $OH^\bullet$). To this end we have forced a triplet solution for the system. However, the total energy is higher than that of the ground state singlet solution described above, where an oxygen displacement from the surface occurs.

3.2 Effect of ZrO_2 catalyst pre-reduction

Experiments show the beneficial effect of catalyst pre-reduction in hydrogen for the ketonization process [8,18,19,20]. As mentioned above, however, the formation of a surface oxygen vacancy on t-ZrO_2 has a cost as large as 6 eV [38]. This value does not change significantly if one considers O vacancies formed at steps sites [38], which seems to contrast the possibility to reduce the zirconia surface by simple O_2 desorption. However, much lower formation energies, in the range of about 3 eV, have been computed for stoichiometic ZrO_2 nanoparticles pointing to an important role of nanostructuring in this context [58]. An alternative path to reduction implies the adsorption and splitting of a hydrogen molecule, the hydrogenation of the surface, and the subsequent removal of water with formation of O vacancies. We discuss in some more detail this latter process, as the other mechanisms have been discussed in separated studies [44].

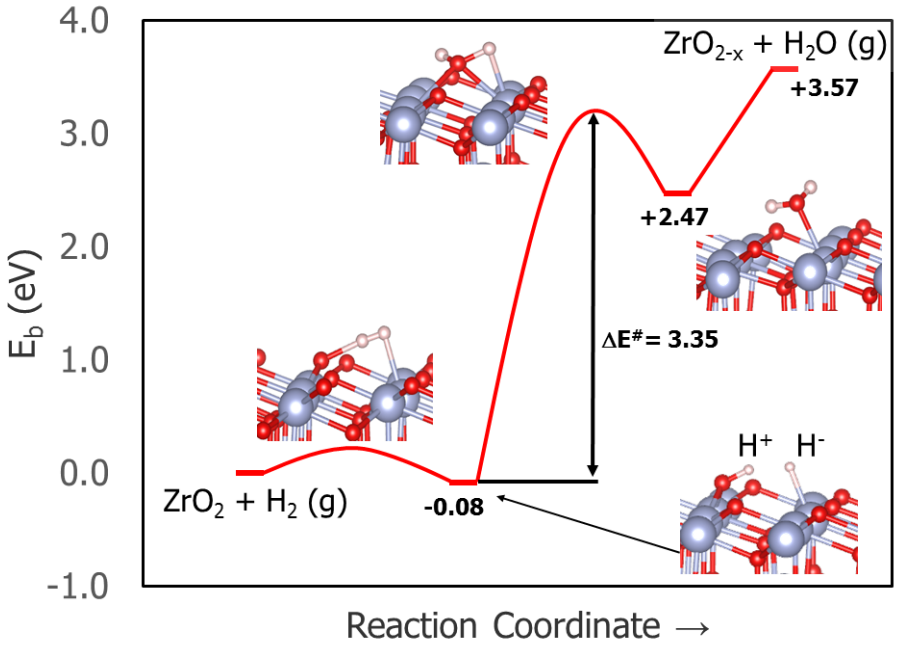

Fig. 2. Energy profile for hydrogenation, formation of adsorbed water, and water desorption with creation of a surface oxygen vacancy on the t-ZrO_2 (101) surface. Blue: Zr; red: O; white H. Energies in eV.

As shown in Figure 2, the splitting of the hydrogen molecule is a slightly exothermic process (-0.08 eV), with an activation energy of 0.24 eV. This leads to the formation of a proton, H^+, bound to an O^{2-} ion, and an hydride, H^-, bound to a Zr^{4+} center (heterolytic dissociation). Notice that a different path is found on zirconia nanoparticles where H_2 dissociates homolytically, with formation of two protons and two Zr^{3+} centers [43]. No matter how hydrogenation occurs, via homolytic or heterolytic splitting, once the surface is hydroxylated another mechanism that may lead to zirconia reduction is water desorption. This process has been followed on the (101) surface, Fig. 2. We find that the formation of an adsorbed water molecule and an O vacancy starting from the hydroxylated surface is endothermic (+2.47 eV) and implies a barrier as large as 3.35 eV. Once formed, the water molecule can easily desorb in gas-phase with a cost of 1.10 eV, leaving a neutral oxygen vacancy on the surface of t-ZrO_2. Using a Redhead equation for first-order desorption processes [59], $\Delta E_{des} = RT_{des} (\ln \nu T_{des} - 3.64)$, and using a pre-factor $\nu = 10^{13}$ s^{-1}, one can conclude that thermal desorption of water is possible for temperatures around 400 K, well below those used in ketonization processes. Furthermore, one should mention that the value of 1.10 eV represents an upper limit since lower desorption energies are expected in correspondence of low-coordinated sites

present on oxide nanoparticles. The final enthalpy cost of O vacancy formation via water desorption, 3.57 eV, is still very high but much lower than that computed for direct O removal via formation of an O_2 molecule, about 6 eV. Also in the case of O vacancy formation via water desorption the entropy contribution can be estimated as done for the adsorption of the gas-phase acetic acid molecule (see § 3.1). Assuming T = 573 K, we obtain a $T\Delta S_{des}$ contribution of -0.85 eV, which results in a ΔG_{des} = 2.72 eV. If we consider that in zirconia nanoparticles the cost of formation of O vacancies by O_2 desorption is strongly reduced with respect to the bare (101) surface [58], we may expect that also water desorption can occur at milder conditions, leaving behind a highly reduced zirconia nanoparticle.

Thus, the hydrogen pre-treatment of the catalyst in the presence of supported metal particles (e.g. Ru) on t-ZrO_2 proceeds via the following steps: hydrogen adsorption and spillover [44], hydroxylation of the surface of the oxide nanoparticle, and possible final desorption of water with formation of O vacancies (at temperatures around 300 °C, the temperature normally used in hydrogen pre-treatment [19]). Notice that while the bulk redox ability of ZrO_2 is much lower than that of other reducible oxides, the ketonization activity may be related to the capability to form vacancies at low-coordinated surface sites more than to the bulk reducibility of the oxide. Another proof in favour of a role of surface O vacancies is that it has been reported that the ketonization activity on a TiO_2 catalyst drops when the reduced catalyst is exposed to O_2 before reaction [19].

The formation of O vacancies is only one way to reduce the zirconia surface, and implies a change in Zr:O ratio (ZrO_{2-x}). Another way to produce reduced centers is via hydrogenation of zirconia when this leads to direct reduction of the oxide via formation of OH^- groups and low-coordinated Zr^{3+} ions. In this case the Zr:O ratio is not modified, and the reduction occurs by electrons addition and not by oxygen removal. We have shown recently that this is the thermodynamically preferred process when zirconia is prepared in form of nanoparticles [43].

In the following we consider the effect of these two different reduction mechanisms on the ketonization reaction, (a) H adsorption and formation of Zr^{3+} ions, and (b) O removal, and formation of O vacancies (morphological defects).

3.3 t-ZrO_2 (101) surface reduced by H addition

In this section we consider the reaction of acetic acid assuming that the hydrogen pre-treatment resulted in the formation of exposed Zr^{3+} ions. The influence of the reduced metal centre on the enolization reaction has been simulated adsorbing the acetate and enolate species discussed above on the surface where an H atom has been added (formation of OH^- and Zr^{3+} centers located on the

surface, Fig. 3). However, neither for the acetate (E_b = -2.32 eV on the reduced surface, E_b = -2.34 eV on non-reduced ZrO_2), nor for the enolate (E_b= -1.79 eV on the reduced surface, E_b = -1.90 eV on non-reduced ZrO_2) we observe a significant change in binding energy as a consequence of the presence of the Zr^{3+} centre. For this reason, the acetate-enolate transition state and activation barrier have not been considered explicitly as they are expected to be similar as on the non-reduced surface. In short, the presence of Zr^{3+} ions (reduced surface by H addition) does not seem to have an effect on the formation of the intermediate 1, enolate (step b1, Scheme 1).

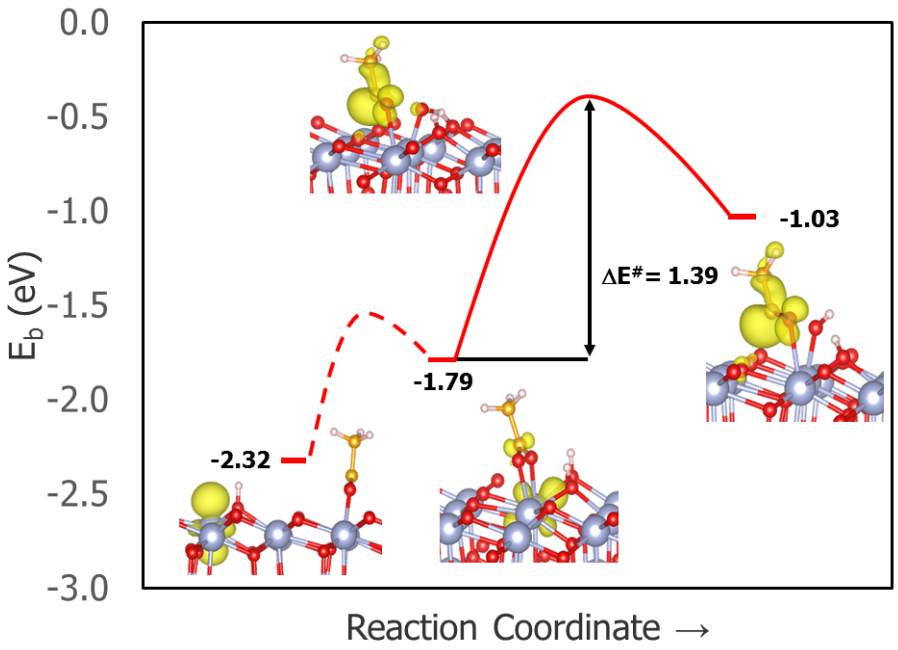

Fig. 3. Energy profile of the formation of the acyl species on hydrogenated t-ZrO_2. The yellow contour shows the spin density. Blue: Zr; red: O; yellow: C; white H. Energies in eV (computed with respect to a gas-phase acetic acid molecule).

Things are different when we consider the effect of the reduced Zr^{3+} centre on the formation of the acyl fragment. As shown in Fig. 3, there is a moderate cost (+0.53 eV) to move the acetate species adsorbed on the surface (E_b= -2.32 eV) close to the Zr^{3+} ion (E_b= -1.79 eV). Then, with a concerted step, the C-O carboxylic bond is broken and the oxygen from the molecule binds a surface proton, with an activation energy of +1.39 eV, forming an acyl radical species stabilized on the surface, $CH_3CO^{\bullet}$. The radical nature of intermediate 2 is proven by the spin density contour,

Fig. 3, that shows that the unpaired electron has moved from the Zr^{3+} ion to the acyl fragment. In this respect, while the formally positively charged CH_3CO^+ species shown in Scheme 1, b2, is unstable on the non-reduced surface (see above), it can form as a radical species by capturing one electron from the reduced surface ($Zr^{3+} \rightarrow Zr^{4+}$). The formation of the acyl radical from CH_3COO^- is uphill by 0.76 eV but leads to a local minimum on the potential energy surface. In this minimum the surface fragments are 1.03 eV more stable than a gas-phase acetic acid molecule, Fig. 3.

Thus, differently from what found for the non-reduced surface, in presence of a Zr^{3+} centre it is possible to stabilize the reactive acyl intermediate in radical form. This shows the importance of these kind of centres for the reactivity of the zirconia surface.

3.4 t-ZrO_{2-x} (101) surface reduced by surface oxygen vacancy

If the surface displays a point defect, such as an oxygen vacancy, there is an important effect on the reaction of the acetate precursor. We start by considering the acetate ion adsorbed close, but not above, the O vacancy. In this configuration, the adsorption energy (E_b= -2.20 eV on ZrO_{2-x}, Fig. 4) is similar to that found on stoichiometric ZrO_2 (E_b= -2.34 eV, Fig. 1). On the contrary, a very large stabilization is found for the enolate species (intermediate 1) forms near an oxygen vacancy (E_b= -3.26 eV on ZrO_{2-x}, -1.90 eV on stoichiometric ZrO_2). Thus, in presence of the defect, the reaction product is stabilized by 1.06 eV with respect to the reactant, leading to an exothermic reaction. The H atom from the methyl group of the acetate is transferred to the vacancy where it forms an hydride H^- ion thanks to the excess electrons associated to the vacancy (as confirmed by the Bader charge on H, -0.63 |e|). A similar effect was reported on monoclinic zirconia [60]. The structural parameters of the enolate ion (C-C bond 1.40 Å, C-O bonds 1.32 and 1.34 Å, H-C-H angle 118°) and the Bader charge (-1.33 |e|) are close to what observed on the stoichiometric surface and indicate the formation of an anionic fragment, CH_2COO^{2-}. However, the energy barrier for the enolization reaction is very small compared to the stoichiometric surface, being of 0.53 eV only, Fig. 4(a). The transition state is characterized by a proton shared between the terminal carbon of the acetate and the oxygen vacancy; d(Zr-H) = 2.08 Å, d(C-H) = 1.34 Å, d(C-C) = 1.45 Å, are similar to what reported for the transition state on the stoichiometric surface.

The whole reaction is:

$$CH_3COOH_{(g)} + V_O^0 \rightarrow CH_3COO^-_{(ads)} + H^+_{(ads\ O)} + V_O^0 \rightarrow CH_2COO^{2-}_{(ads)} + H^+_{(ads\ O)} + V_O^{2+}/(H^-) \quad (1)$$

and implies an overall energy gain of 3.26 eV with respect to the reduced surface and a gas-phase acetic acid molecule, Fig. 4(a).

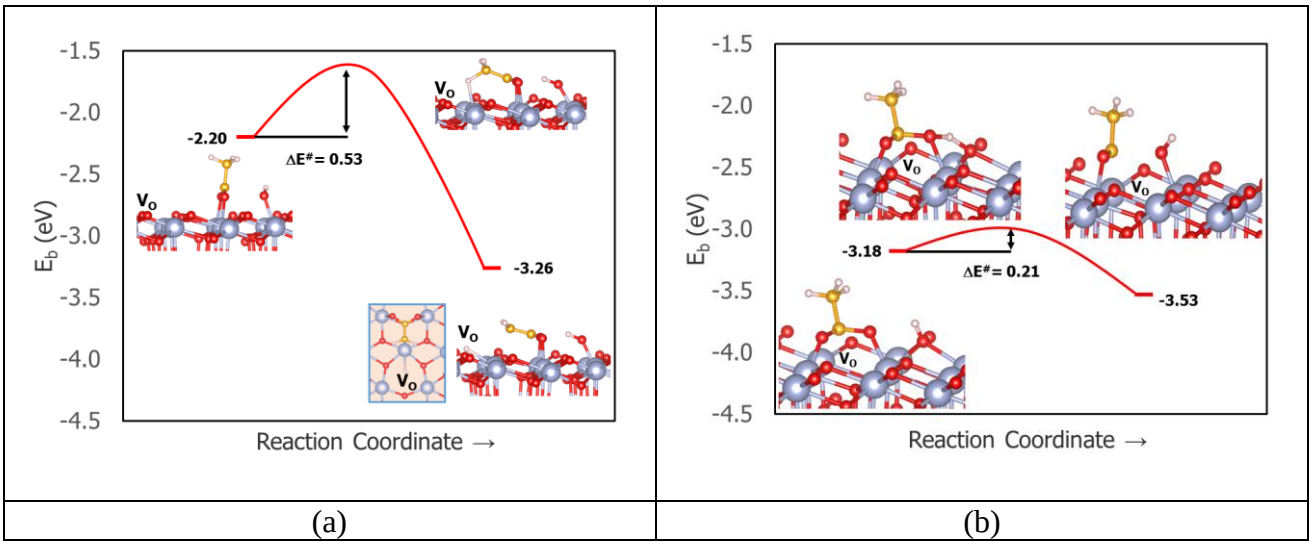

(a) (b)

Fig. 4. (a) Energy profile of the enolization reaction on t-ZrO_{2-x} in presence of a surface oxygen vacancy. (b) Formation of the acyl species on t-ZrO_{2-x} in presence of a surface oxygen vacancy. Blue: Zr; red: O; yellow: C; white H. Energies in eV (computed with respect to a gas-phase acetic acid molecule).

The other step is the formation of the acyl species (intermediate 2, Scheme 1, b2). Also in this case, the presence of a surface vacancy is of great relevance. Here we consider as a starting structure an acetate ion adsorbed on top of an oxygen vacancy and a proton adsorbed on an O ion (CH_3COO^- + H^+), Fig. 4(b). This structure displays a stability of -3.18 eV with respect to the surface with an O vacancy and gas-phase CH_3COOH. The deoxygenation of the acetate moiety leads to a negatively charged CH_3CO^- unit (Bader charge -0.65 |e|) and an OH^- group adsorbed on a Zr ion. The entire process can be seen as the result of the homolytic cleavage of CH_3COOH into $CH_3CO^\bullet$ and $OH^\bullet$ radicals, followed by the transfer of the two excess electrons associated to the vacancy to the two radicals with formation of two stable anionic CH_3CO^- and OH^- species:

$$CH_3COOH_{(g)} + V_O^0 \rightarrow CH_3COO^-_{(ads)} + H^+_{(ads\ O)} + V_O^0 \rightarrow CH_3CO^-_{(ads)} + OH^-_{(ads\ Zr)} + V_O^{2+} \quad (2)$$

This is an important result. In fact, while this step is not possible on the bare zirconia surface and is endothermic by 0.76 eV on the hydrogenated t-ZrO_2 surface, in presence of an O vacancy it becomes exothermic by 0.35 eV, Fig. 4(b). Also the activation barrier is rather small, 0.21 eV, leading to an overall easy process.

Reaction (2) implies an overall energy gain of 3.53 eV with respect to the reduced surface and a gas-phase acetic acid molecule. This energy gain is comparable to that found for the reaction (1) described above (-3.26 eV). Also the barriers for the two reactions, 0.21 and 0.53 eV, are similar and small. Given the various approximations inherent to the models used, the two processes can be considered to be competitive and to occur with similar probability. The alternative is that the acetate ions diffuses on the surface and reacts preferentially with the O vacancies where is more strongly bound. In this scenario, the acyl anion forms in the presence of the O vacancies and then reacts with the enolate species formed on regular sites of the surface. Only a microkinetic model could answer these questions, but again the conclusions would strongly depend on the input parameters and the energy profiles for the two scenarios are relatively similar.

3.5 Ketonization on the reduced t-ZrO (101) surface

The next step in the reaction is the combination of the two intermediates 1 and 2 to form the β-keto-acid, step c of Scheme 1. We have seen that the reaction mechanism is not easy on the bare zirconia surface since the acyl intermediate is unstable.

In the presence of Zr^{3+} ions (reduction by H addition), the $CH_3CO^{\bullet}$ intermediate 2 is stable and can further react with the enolate ion (intermediate 1) to form the 3-oxo-butyrrate (Fig. 5) which is the precursor of the final product of the ketonization. The process occurs by direct attack of $CH_3CO^{\bullet}$ to the CH_2COO^{2-} unit, Fig. 5, with an activation barrier of 0.4 eV, that can be easily overcome at the temperatures of the reaction. The final structure has a stability of -2.44 eV with respect to the energy of two CH_3COOH gas-phase molecules and the zirconia surface.

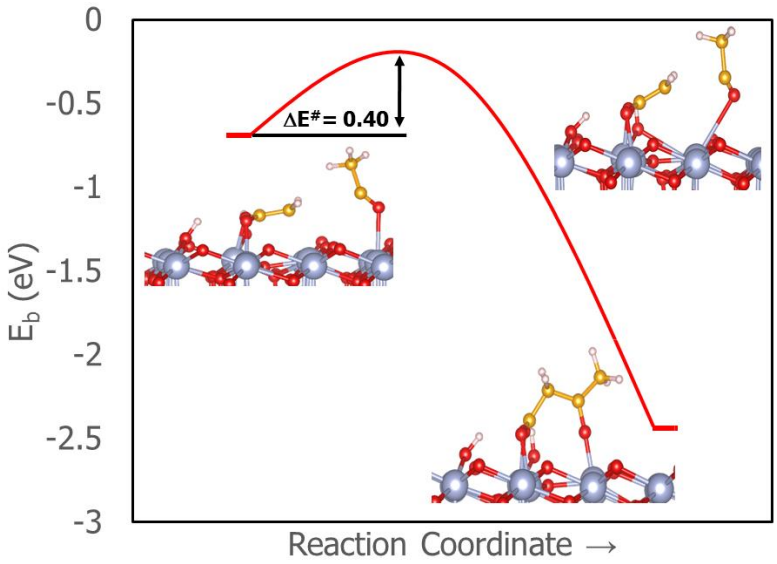

Fig. 5. Formation of the 3-oxo-butyrrate ion on hydrogenated t-ZrO_2. Blue: Zr; red: O; yellow: C; white H. Energies in eV (computed with respect to two gas-phase acetic acid molecules).

In the presence of an O vacancy, the formation of the 3-oxo-butyrrate species has been studied starting from the combination of the acyl anion formed near the vacancy and an enolate moiety (Fig. 6). The two fragments have been adsorbed on the same supercell at close distance. The formation of the β-keto-acid product is, in this case, moderately endothermic by 0.25 eV, with an overall binding energy of -4.04 eV. The kinetic barrier for this step is 1.03 eV.

So, while in the presence of exposed Zr^{3+} cations the process occurs with a small barrier (0.4 eV), on a reduced surface by O vacancies the process implies a somewhat higher barrier, 1.03 eV, still accessible at the reaction temperatures.

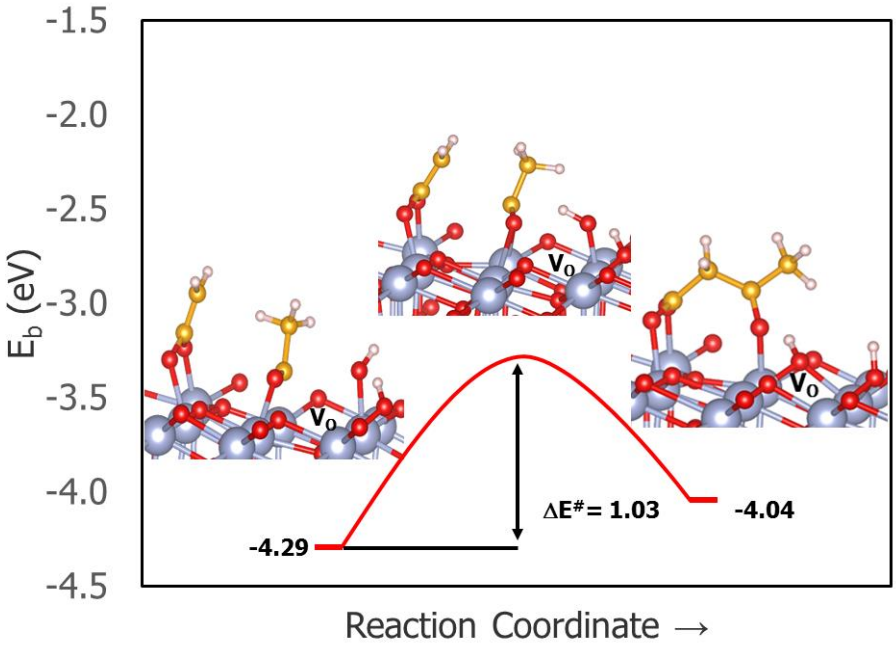

Fig. 6. Formation of the 3-oxo-butyrrate ion on t-ZrO_{2-x} in presence of a surface oxygen vacancy. Blue: Zr; red: O; yellow: C; white H. Energies in eV (computed with respect to two gas-phase acetic acid molecules).

4. Conclusions

In this work, a possible reaction path for the ketonization reaction of acetic acid on tetragonal zirconia has been analysed by means of DFT+U calculations, comparing the properties of a defect-free surface to the cases of a zirconia (101) surface reduced (a) by means of hydrogenation and (b) by creation of an oxygen vacancy. The reaction implies a) adsorption of two acetic acid molecules; b) the formation of the enolate intermediate 1, c) the formation of the acyl intermediate 2, and d) the reaction of acyl and enolate intermediates to form the β-keto-acid. This then releases CO_2 and forms acetone by hydrogen transfer from the surface These last two steps have not been considered here but can be affected as well by the reduction of the surface. The conclusions can be summarized as follows:

- On non-reduced t-ZrO_2, the reaction of the acetate ion to give enolate is hindered by a rather large activation energy. If the same computational method is used, then the activation energy is similar to that reported for the same reaction on on monoclinic zirconia [27]. Even more difficult is the deoxygenation of the acetate fragment, since the acylium cationic

intermediate is unstable and tends to abstract one oxygen ion from the surface, reforming acetate.

- Bulk zirconia is not an easily reducible oxide, as shown by the very large cost of creation of an oxygen vacancy. However, several ways exist to reduce the surface of this oxide, such as hydrogen spillover followed by formation of protons and Zr^{3+} ions, reverse oxygen spillover, or water desorption. All these effects become more relevant on zirconia nanoparticles due to the presence of undercoordinated sites [43,58].

- On hydrogenated (reduced) zirconia, the electron hosted in a Zr^{3+} reduced centre is easily transferred to the acetate ion during the deoxygenation reaction, forming an acyl radical which easily reacts with the enolate fragment to form the β-keto-acid. This shows that the presence of exposed Zr^{3+} ions can be extremely beneficial for the ketonization reaction.

- The presence of a surface oxygen vacancy has a strong impact on the keto-eno tautomeric equilibrium, where the enolate species is strongly stabilized with respect to the acetate fragment. The kinetic barrier is also smaller compared to stoichiometric zirconia. Similarly, in the deoxygenation step we also observe a remarkable stabilization of the reaction intermediate in the form of an anionic acyl species and a strong decrease of the activation energy. The combination of enolate and acyl ions to form the β-keto-acid implies an higher barrier than in the present of Zr^{3+} ions, but is much easier than on the stoichiometric surface.

- What remains to be understood in detail is how the reactive centers are re-generated in the course of the reaction. Zr^{3+} centers are created by the initial pre-treatment of the catalyst in hydrogen and are regenerated after the reactants have transformed into products. More complex is the regeneration of oxygen vacancies. One possible scenario is that they are produced thanks to the water molecules that are released in the course of the ketonization process, see scheme 1c. The presence of water results in an hydroxylated zirconia surface, and the calculations have shown that at the temperatures of the reaction water can desorb from the surface leaving behind oxygen vacancies, in particular in correspondence of low-coordinated sites.

The work highlights at the atomistic level the role and the importance of the zirconia catalyst pre-treatment in hydrogen for the ketonization reaction. The conclusions, obtained for the tetragonal phase of zirconia, are valid also for the monoclinic one and, more generally, for other oxides. While this is not essential as the reaction can occur also on non-reduced surfaces, the pre-reduction

has the overall effect to lower the barriers and stabilize some key intermediates, making the reaction easier.

Acknowledgments

This work has been supported by the European Community's Seventh Framework Programme FP7/2007-2013 under Grant Agreement n° 604307 (CASCATBEL).

[1] W. Q. Shen, G. A. Tompsett, R. Xing, W. C. Conner, G. W. Huber, Vapor phase butanal self-condensation over unsupported and supported alkaline earth metal oxides, J. Catal. 286 (2012) 248−259.
[2] L. Faba, F. Díaz, S. Ordonez, One-pot aldol condensation and hydrodeoxygenation of biomass-derived carbonyl compounds for biodiesel synthesis, ChemSusChem 7 (2014) 2816−2820.
[3] O. Kikhtyanin, D. Kubicka, J. Cejka, Toward understanding of the role of Lewis acidity in aldol condensation of acetone and furfural using MOF and zeolite catalysts, Catal. Today 243 (2015) 158-162.
[4] D. Mohan, C.U. Pittman, P.H. Steele, Pyrolysis of wood/biomass for bio-oil: a critical review, Energy & Fuels 20 (2006) 848-889.
[5] J. M. Clark, M. R. Nimlos, D. J. Robichaud, Comparison of unimolecolar decomposition pathways for carboxylic acids of relevance in biofuels, J. Phys. Chem. A 118 (2014) 260-274.
[6] S. Rajadurai, Pathways for carboxylic acid decomposition on transition metal oxides, Catal. Rev.-Sci. Eng. 36 (1994) 385-403.
[7] R. Martinez, M. C. Huff, M. A. Barteau, Ketonization of acetic acid on titania-functionalized silica monoliths, J. Catal. 222 (2004) 404-409.
[8] T.N. Pham, T. Sooknoi, S.P. Crossley, D.E. Resasco, Ketonization of carboxylic acids: mechanisms, catalysts, and implications for biomass conversion, ACS Catal. 3 (2013) 2456-2473.
[9] G. Pacchioni, Ketonization of carboxylic acids in biomass conversion over TiO_2 and ZrO_2 surfaces: a DFT perspective, ACS Catal. 4 (2014) 2874-2888.
[10] K. S. Kim, M. A. Barteau, Structure and composition requirements for deoxygenation, dehydration, and ketonization reactions of carboxylic acids on TiO_2(001) single-crystal surfaces, J. Catal. 125 (1990) 353-375.
[11] M. A. Barteau, Organic reactions at well-defined oxide surfaces, Chem. Rev. 96 (1996) 1413−1430.
[12] K. Okumura, Y. Iwasawa, Zirconium oxides dispersed on silica derived from Cp_2ZrCl_2, $[(i\text{-}PrCp)_2ZrH(\mu\text{-}H)]_2$, and $Zr(OEt)_4$ characterized by X-ray absorption fine structure and catalytic ketonization of acetic Acid, J. Catal. 164 (1996) 440-448.
[13] V. N. Panchenko, Y. A. Zaytseva, M. N. Simonov, I. L. Simakova, E. A. Paukshtis, DRIFTS and UV-vis DRS study of valeric acid ketonization mechanism over ZrO_2 in hydrogen atmosphere, J. Mol. Catal. A 388-389 (2014) 133-140.
[14] A. V. Ignatchenko, E. I. Kozliak, Distinguishing enolic and carbonyl components in the mechanism of carboxylic acid ketonization on monoclinic zirconia, ACS Catal. 2 (2012) 1555-1562.
[15] A. Pulido, B. Oliver-Tomas, M. Renz, M. Boronat, A. Corma, Ketonic decarboxylation reaction mechanism: A combined experimental and DFT study, ChemSusChem 6 (2013) 141-151.
[16] Y. Lee, J.-W. Choi, D. J. Suh, J.-M. Ha, C.H. Lee, Ketonization of hexanoic acid to diesel-blendable 6-undecanone on the stable zirconia aerogel catalyst, Appl. Catal. A 506 (2015) 288-293.
[17] A. V. Ignatchenko, J. S. DeRaddo, V. J. Marino, A. Marino, A. Mercado, Cross-selectivity in the catalytic ketonization of carboxylic acids, Appl. Catal. A 498 (2015) 10-24.
[18] S. Foraita, J. L. Fulton, Z. A. Chase, A. Vjunov, P. Xu, E. Barth, D. M. Camaioni, C. Zhao, J. A. Lercher, Impact of the oxygen defects and the hydrogen concentration on the surface of tetragonal and monoclinic ZrO_2 on the reduction rates of stearic acid on Ni/ZrO_2, Chem. Eur. J. 21 (2015) 2423-2434.
[19] T. N. Pham, D. Shi, D. E. Resasco, Kinetics and mechanism of ketonization of acetic acid on Ru/TiO_2 catalyst, Top. Catal. 57 (2014) 706-714.

[20] T. N. Pham, D. Shi, T. Sooknoi, D. E. Resasco, Aqueous-phase ketonization of acetic acid over Ru/TiO_2/carbon catalysts, J. Catal. 295 (2012) 169-178.
[21] L. Rand, W. Wagner, P.O. Warner, L.R. Kovac, Reactions Catalyzed by Potassium Fluoride. II. The Conversion of Adipic Acid to Cyclopentanone, J. Org. Chem. 27 (1962) 1034-1035.
[22] M. Renz, Ketonization of carboxylic acids by decarboxylation: mechanism and scope, Eur. J. Org. Chem. (2005) 979-988.
[23] O. Neunhoeffer, P. Paschke, Über den Mechanismus der Ketonbildung aus Carbonsäuren, Ber. Dtsch. Chem. Ges. A/B 72 (1939) 919-929.
[24] R. Pestman, R. M. Koster, A. van Duijne, J. A. Pieterse, V. Ponec, Reactions of carboxylic acids on oxides. 2. Bimolecular reaction of aliphatic acids to ketones, J. Catal. 168 (1997) 265-272.
[25] A. Gumidyala, T. Sooknoi, S. Crossley, Selective ketonization of acetic acid over HZSM-5: the importance of acyl species and the influence of water, J. Catal. 340 (2016) 76-84.
[26] L. K. Dash, N. Vast, P. Baranek, M. C. Cheynet, L. Reining, Electronic structure and electron energy-loss spectroscopy of ZrO_2 zirconia, Phys. Rev. B 70 (2004) 245116.
[27] A.V. Ignatchenko, Density functional theory study of carboxylic acids adsorption and enolization on monoclinic zirconia surfaces, J. Phys. Chem. C 115 (2011) 16012-16018.
[28] S. Shukla, S. Seal, Mechanisms of room temperature metastable tetragonal phase stabilisation in zirconia, Int. Mater. Rev. 50 (2005) 45-64.
[29] X. Guo, Low temperature stability of cubic zirconia, Phys. Status Solidi A 177 (2000) 191-201.
[30] E. V. Stefanovich, A. L. Shluger, C. R. A. Catlow, Theoretical study of the stabilization of cubic-phase ZrO_2 by impurities, Phys. Rev. B 49 (1994) 11560.
[31] A. Dwivedi, A. N. Cormack, A computer simulation study of the defect structure of calcia-stabilized zirconia, Philos. Mag. 61 (1990) 1-22.
[32] V. V. Kharton, F. M. B. Marques, A. Atkinson, Transport properties of solid oxide electrolyte ceramics: a brief review, Solid State Ion. 174 (2004) 135-149.
[33] A. A. Shutilov, M. N. Simonov, Yu. A. Zaytseva, G. A. Zenkovets, and I. L. Simakova, Phase composition and catalytic properties of ZrO_2 and CeO_2-ZrO_2 in the ketonization of pentanoic acid to 5-nonanone, Kin. Catal. 54 (2013) 184-192.
[34] Y. A. Zaytseva, V. N. Panchenko, M. N. Simonov, A. A. Shutilov, G. A. Zenkovets, M. Renz, I. L. Simakova, V. N. Parmon, Effect of gas atmosphere on catalytic behaviour of zirconia, ceria and ceria-zirconia catalysts in valeric acid ketonization, Top. Catal 56 (2013) 846-855.
[35] B. Peng, C. Zhao, S. Kasakov, S. Foraita, J. A. Lercher, Manipulating catalytic pathways: deoxygenation of palmitic acid on multifunctional catalysts, Chem. Europ. J. 19 (2013) 4732-4741.
[36] A. Hofmann, S.J. Clark, M. Oppel, I. Hahndorf, Hydrogen adsorption on the tetragonal ZrO_2(101) surface: a theoretical study of an important catalytic reactant, Phys. Chem. Chem. Phys. 4 (2002) 3500-3508.
[37] H.Y.T. Chen, S. Tosoni, G. Pacchioni, A DFT study of the acid-basic properties of anatase TiO_2 and tetragonal ZrO_2 by adsorption of CO and CO_2 probe molecules, Surf. Sci. 652 (2016) 163-171.
[38] S. Tosoni, H.Y.T. Chen, G. Pacchioni, A DFT study of the reactivity of anatase TiO_2 and tetragonal ZrO_2 stepped surfaces compared to the regular (101) terraces, ChemPhysChem 16 (2015) 3642-3651.
[39] V. Ganduglia-Pirovano, A. Hofmann, J. Sauer, Oxygen vacancies in transition metal and rare earth oxides: Current state of understanding and remaining challenges, Surf. Sci. Rep. 62 (2007) 219-270.
[40] H.Y.T. Chen, S. Tosoni, G. Pacchioni, Adsorption of ruthenium atoms and clusters on anatase TiO_2 and tetragonal ZrO_2(101) surfaces: A comparative DFT study, J. Phys. Chem. C 119 (2014) 10856-10868.
[41] S. Tosoni, H.Y.T. Chen, G. Pacchioni, A DFT study of Ni clusters deposition on titania and zirconia (101) surfaces, Surf. Sci. 646 (2016) 230-238.
[42] C. Gionco, M. C. Paganini, E. Giamello, R. Burgess, C. Di Valentin, G. Pacchioni, Paramagnetic defects in polycrystalline zirconia: an EPR and DFT study, Chem. Mater. 25 (2013) 2243-2253.
[43] A. Ruiz, S. Tosoni, G. Pacchioni, Turning a non-reducible into a reducible oxide via nanostructuring: opposite behaviour of bulk ZrO_2 and ZrO_2 nanoparticles towards H_2 adsorption, J. Phys. Chem. C, 120 (2016) 15329–15337.
[44] H.Y.T. Chen, S. Tosoni, G. Pacchioni, Hydrogen adsorption, dissociation, and spillover on Ru_{10} clusters supported on anatase TiO_2 and tetragonal ZrO_2 (101) surfaces, ACS Catal. 5 (2015) 5486-5495.

[45] G. Kresse, J. Furthmüller, Efficiency of ab-initio total energy calculations for metals and semiconductors using a plane-wave basis set, J. Comput. Mater. Sci. 6 (1996) 15-50.
[46] J. P. Perdew, K. Burke, M. Ernzerhof, Generalized gradient approximation made simple, Phys. Rev. Lett. 77 (1996) 3865-3868.
[47] P. E. Blöchl, Projector augmented-wave method, Phys. Rev. B 50 (1994) 17953-17979.
[48] G. Kresse, J. Joubert, From ultrasoft pseudopotentials to the projector augmented-wave method, Phys. Rev. B 59 (1999) 1758-1775.
[49] V. I. Anisimov, J. Zaanen, O. K. Andersen, Band theory and Mott insulators: Hubbard U instead of Stoner I, Phys. Rev. B 44 (1991) 943-954.
[50] S. L. Dudarev, G. A.Botton, S. Y. Savrasov, C. J. Humphreys, A. P.Sutton, Electron-energy-loss spectra and the structural stability of nickel oxide: An LSDA+U study, Phys. Rev. B 57 (1998) 1505-1509.
[51] S. Grimme, Semiempirical GGA-type density functional constructed with a long-range dispersion correction, J. Comput. Chem. 27 (2006) 1787-1799.
[52] A. Ruiz, P. Schlexer, G. Pacchioni, Gold and silver clusters on TiO_2 and ZrO_2 (101) surfaces: role of dispersion forces, J. Phys. Chem. C 119 (2015) 15381−15389.
[53] G. Mills, H. Jonsson, G. K. Schenter, Reversible work transition state theory: application to dissociative adsorption of hydrogen, Surf. Sci. 324 (1995) 305-337.
[54] H. Jónsson, G. Mills aK. W. Jacobsen, `Nudged elastic band method for finding minimum energy paths of transitions', in: B. J. Berne, G. Ciccotti, D. F. Coker (Eds.), Classical and quantum dynamics in condensed phase simulations, World Scientific, London, 1998, p. 387.
[55] G. Henkelman, H. Jónsson, A climbing image nudged elastic band method for finding saddle points and minimum energy paths, J. Chem. Phys. 113 (2000) 9901-9904.
[56] J. K. Norskov, F. Studt, F. Abild-Pedersen, T. Bligaard, Fundamental Concepts in Heterogeneous Catalysis, John Wiley & Sons, Hoboken, 2014, p. 1-196.
[57] S. Posada-Perez, P. J. Ramirez, J. Evans, F. Vines, P. Liu, F. Illas, J. A. Rodriguez, Highly Active Au/delta-MoC and Cu/delta-MoC Catalysts for the Conversion of CO_2: The Metal/C Ratio as a Key Factor Defining Activity, Selectivity, and Stability, J. Am. Chem. Soc. 138 (2016) 8269-8278.
[58] A. Ruiz, F. Illas, G. Pacchioni, Structure and properties of zirconia nanoparticles from density functional theory calculations, J. Phys. Chem. C 120 (2016) 4392–4402.
[59] a) P. A. Redhead, Thermal desorption of gases, Vacuum 12 (1962) 203-211; b) K. Christmann, 'Introduction to Surface Physical Chemistry', Springer, 1991, p. 156.
[60] O.A. Syzgantseva, M. Calatayud, C. Minot, Revealing the surface reactivity of zirconia by periodic DFT calculations, J. Phys. Chem. C 116 (2012) 6636-6644.